Journal of Physics: Conference Series **500** (2014) 012001 doi:10.1088/1742-6596/500/1/012001

Unusual behaviour of usual materials in shock waves

G I Kanel

Joint Institute for High Temperatures of Russian Academy of Sciences, Izhorskaya 13, bld. 2, Moscow, 125412 Russia

kanel@ficp.ac.ru

Abstract. Exotic results of investigations of inelastic deformation and fracture under shock wave loading are presented and briefly discussed. Temperature effects on the flow stress at high strain rate may differ even in sign from those we observe at low and moderate strain rates. Investigations of the temperature-rate dependence of the yield stress at shock compression demonstrate intense multiplication of dislocations. At the highest strain rates, so-called ideal (ultimate) shear and tensile strength is reached in experiments with picosecond durations of shock loading. Although grain boundaries, in general, reduce resistance to fracture as compared to single crystals, the spall strength of ultra-fine-grained metals usually slightly exceeds that of coarse-grain samples. Failure wave phenomena have been observed in shock-compressed glasses.

1. Introduction

The early investigations of shock compression of condensed matter were stimulated by the practical necessity of obtaining the equations of state in the megabar pressure range. However, shock-wave experiments are characterized not only by high attainable pressure and temperature, but also by very small load durations and extremely high rates of the load application. The shock-wave techniques provide the unique capabilities to study such time-dependent phenomena as inelastic deformation, fracture, phase transitions, etc. Under these conditions, the exotic and unpredicted behavior of some materials has been observed.

Modern progress in investigations into high-rate deformation, fracture, and physicochemical transformations in shock waves has been provided by the development of techniques for measuring wave profiles with a high temporal resolution. The time resolution of the widely used VISAR [1] and ORVIS [2] velocimeters is around one nanosecond. The time range available for shock-wave measurements has been recently expanded to picoseconds [3,4] by development of precise displacement interferometer techniques with femtosecond lasers. The varying of the test temperature significantly broadened the range of the processes and effects under investigation [5,6].

Figures 1 and 2 show the examples [6,7] of such measurements for iron samples. The shock wave in iron splits into two or three compression waves. The first one is the elastic precursor wave. The stress at it is the Hugoniot elastic limit (HEL). It is seen from the figures that the recorded HEL value varies with the temperature and the propagation distance. At 250 nm of the sample thickness the recorded HEL value is as large as 27.5±2.5 GPa. At highest HEL value, a deflection from equilibrium state $\sigma_x - p$ = 10.5 GPa. The observations of such large deflections should stimulate theoretical analysis of strongly metastable Hugoniots and isentropes of uniaxial compression. The HEL of iron decreases with increasing the temperature as it occurs at low and moderate strain rates. It will be

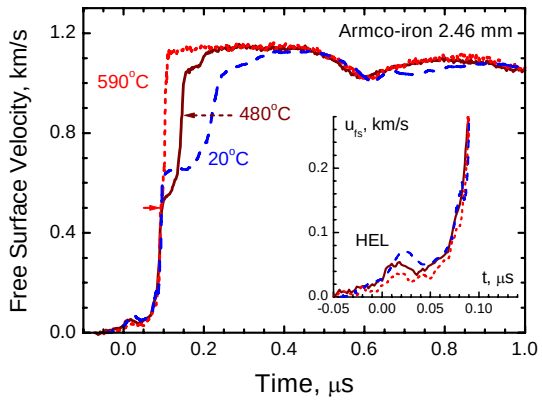

Figure 1. The free surface velocity histories of the Armco iron samples 2.46 mm in thickness impacted at various temperatures [6].

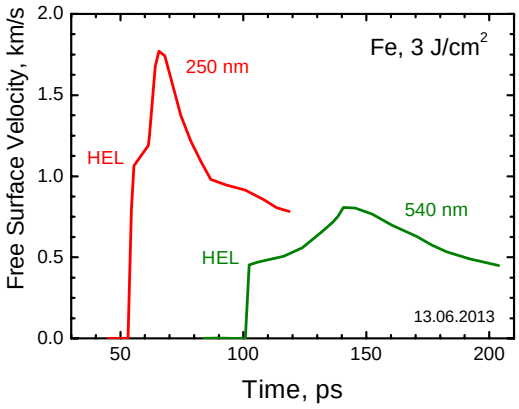

Figure 2. The free surface velocity histories of iron films 250 nm and 540 nm in thickness heated by laser pulse of 100 fs duration [7].

shown below that in some cases there is an anomalous increase of the HEL instead of its decrease at heating.

In most cases, but by no means always, the sub-microsecond behavior of materials corresponds to that expected on the basis of extrapolation from the larger time interval and the smaller strain rates. However, sometimes we see anomalous deflection from extrapolation which could be expected but was not predicted by theories. In this review we present new and unexpected results of the investigations into the strength properties of metals and alloys under submicrosecond-long shock-wave loading, the observations of deeply metastable states of materials and the studying of their mechanical behavior at extremely high strain rates.

2. Rate and temperature effects on the flow stress of metals

It is well known that the flow stress of crystalline solids increases with an increase in the strain rate. For many metals, this dependence sharpens when the rate of deformation exceeds ~10^3–10^4 s^{-1}, which is interpreted as the consequence of the change in a mechanism of dislocations motion [10,11]. At low strain rates, dislocations overcome obstacles due to the joint action of the applied stress and thermal fluctuations. Because of this, the increase of temperature is accompanied by the decrease in the yield strength of materials. For sufficiently high strain rates, the dominant drag mechanism becomes phonon friction. As the phonon friction is proportional to the temperature, for very high strain rates, one can expect an increase in the flow stress with an increase in temperature [12] as it is shown in figure 3. At some stress, which is termed the "ideal" or "ultimate" shear strength, the material loses its shear stability and may be deformed without any contribution of dislocations. The value τ_{id} of the ideal shear strength is proportional to the shear modulus value G: $\tau_{id} \approx G/10 \ldots G/2\pi$. Since the shear modulus decreases with the temperature, the ideal strength decreases with heating as well.

There are two direct (without computer simulations) ways to get information about the relationships between the plastic strain rate and the flow stress: the measurements of the decay of the elastic precursor wave [13,14] and the measurements of the rise time of the plastic shock wave [15,16]. Figure 4 [17,18] summarizes experimental data for commercial and pure aluminum. The HEL value varies from 50 MPa at 10 mm up to 20.5 GPa at 1.2 μm of propagation distance. Such large compression causes significant nonlinear effects for the deviatoris stresses. With the obtained empirical elastic precursor decay, we finally have the initial plastic strain rate as a function of shear stress for aluminum: $\dot{\gamma}_p = 9.1\times10^7(\tau/\tau_0)^{2.59}$ s^{-1}, where $\tau_0 = 1$ GPa. The plastic strain rate decreases

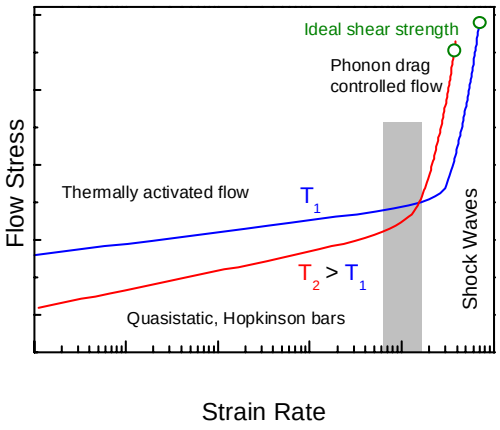

Figure 3. General time–temperature dependences of the yield stress.

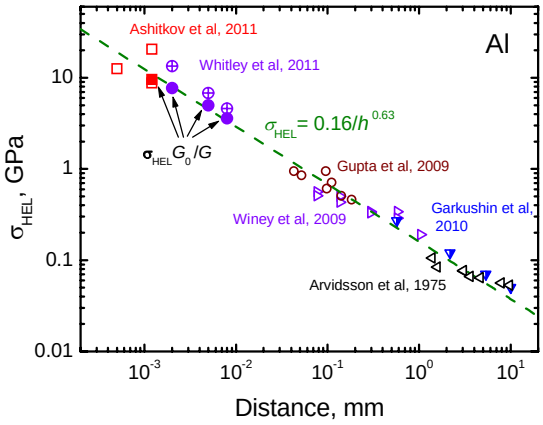

Figure 4. Decay of the elastic shock wave in pure or commercially pure aluminum [17].

from 10^9 s^{-1} after 1 μm of the propagation distance to 10^3 s^{-1} at 5-10 mm. At 10 mm of the distance, the decay of HEL sharply decelerates.

Figure 5 compares the low-rate and the high-rate branches of the total flow stress dependence on the strain rate for aluminum. For harder aluminum alloys, the low-rate branch intersects the high-rate branch at higher stresses and higher strain rates.

Figure 6 shows the free surface velocity histories of monocrystalline aluminum specimens measured under shock-wave loading at different temperatures [19,20]. Directly from these profiles one can see that the HEL rises significantly with increasing temperature, i.e. the dynamic yield stress increases. Such an anomalous growth of the dynamic yield stress with increasing temperature is caused by the transition to phonon friction as the main dislocation drag mechanism at high strain rate and was observed for several crystalline materials.

Figure 7 presents an example of the measured temperature-rate dependencies of the yield stress for pure polycrystalline aluminum under the shock compression conditions [21]. The data include states at the HEL and in the plastic shock wave. The comparison of the data presented in figure 7 shows that the plastic strain rate in shock wave is larger by order of magnitude than that in elastic precursor at the same shear stress. Faster plastic deformation requires more mobile dislocations: intense multiplication of dislocations occurs behind the elastic wave front.

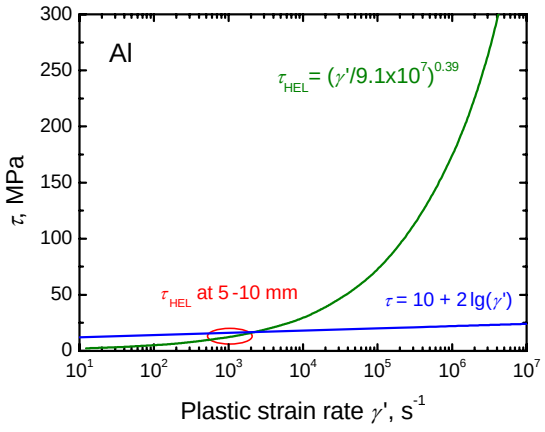

Figure 5. Rate sensitivity of the flow stress in aluminum.

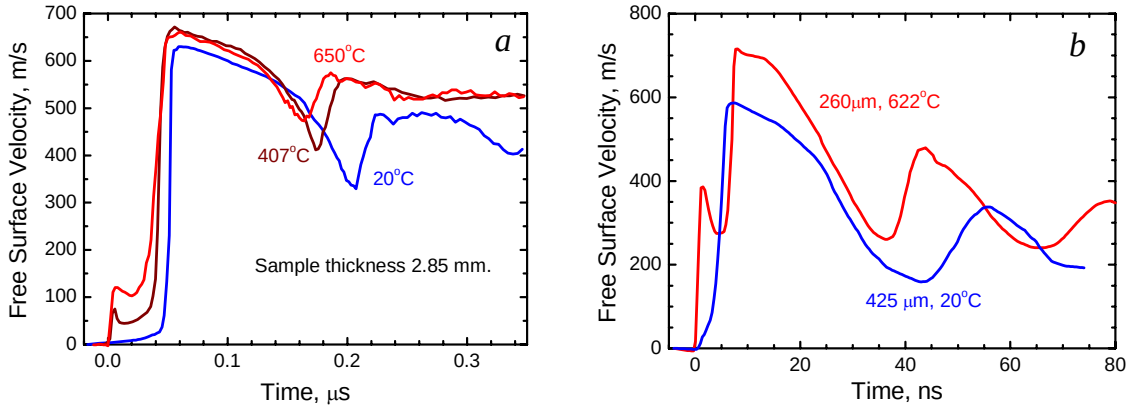

Figure 6. Free surface velocity histories for monocrystalline aluminum specimens of different thicknesses. The test temperature is shown for the wave profiles. (*a*) Results of experiments with planar impactors [19], (*b*) generation of short compression pulses by an ion beam [20].

Figure 8 presents experimental data on the decay of the elastic precursor wave in annealed aluminum alloy 6061 at 300 and 851 K in comparison with the dependence at the $\sigma_{HEL}(h)$ for pure aluminum [21]. In some cases the harder alloy exhibits even a smaller HEL than pure aluminums that certainly is associated with different initial densities of mobile dislocations and different rates of their nucleation and multiplication.

It has been shown by several observations of the elastic precursor decay that the values of densities of mobile dislocations which are required to provide the observed initial plastic strain rates at the HEL are much larger than the usual total densities of dislocations in pure annealed metals. In each of these studies, it was assumed that any plastic deformation does not occur and the dislocation density remains unchanged through the front part of the elastic precursor. However, this assumption is probably not true. Figure 9 shows the evolution of waveforms of shock compression of pure copper with increasing temperature [22]. Increase in the HEL value causes decrease of the rise time of the elastic precursor wave. Approaching the shortest rise time of the elastic shock is accompanied by a change of the wave

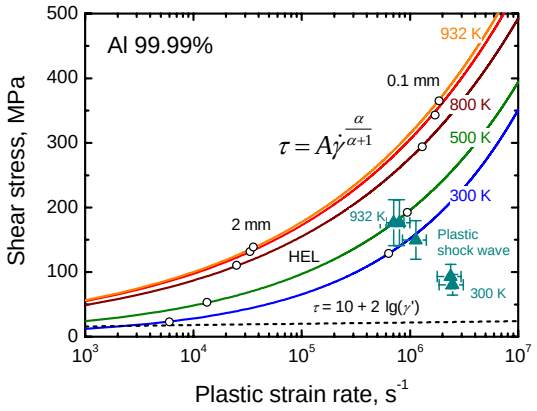

Figure 7. The shear stress τ at the HEL as a function of plastic strain rate $\dot{\gamma}$ in pure aluminum shocked at different temperatures. The triangles with error bars are the points corresponding to plastic shock waves [21].

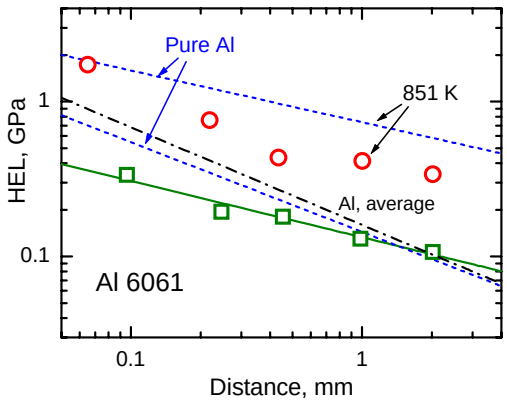

Figure 8. Decay of the elastic precursor wave in annealed 6061 aluminum at room temperature and 851 K in comparison with decay in pure aluminum at the same temperatures [21]. The dash-dotted line presents approximation of entire volume of data for various aluminums.

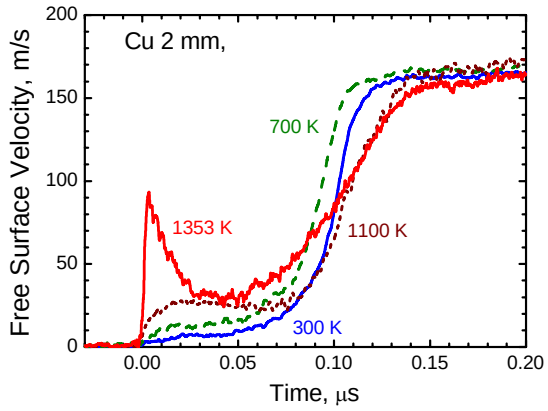

Figure 9. Front parts of the free surface velocity histories of pure copper samples impacted at various temperatures [22].

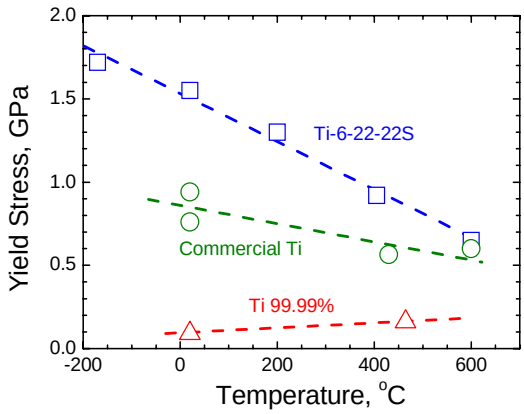

Figure 10. Temperature dependencies of dynamic yield strengths of Ti-6-22-22S alloy, commercial grade titanium, and titanium of 99.99% purity [23].

shape which probably means the displacement of the dislocation multiplication from the dispersed elastic shock compression wave to the space behind it.

Figure 10 compares the temperature dependencies of the dynamic yield stress for titanium and its two alloys [23]. The measured data show an anomalous rise in dynamic yield stress under the shock compression of soft high-purity titanium, while the behavior of high-strength alloys is similar to that under the ordinary conditions at low strain rates. In a pure metal the flow stress is not high and is comparable to the forces of phonon friction, and their increase with rising temperature therefore makes a significant contribution to the dislocation drag forces. Alloys always contain numerous obstacles in the form of impurities and interfaces which are purposely introduced to increase the flow stress. The stresses required to overcome these obstacles far exceed the phonon frictional forces.

3. Spall fracture of metals

The dynamic tensile strength of materials at load durations of a few microseconds or less is studied by analyzing the spall phenomena under shock pulse loading. The high-rate fracture at spalling is a kinetic process of nucleation, growth, and coalescence of numerous micro-voids or micro-cracks. As a result the limited rates of these processes, the realized values of the resistance to fracture increase with increase of the rate of applying the load.

The tensile stress value just before spalling, spall strength σ_{sp}, is proportional to the velocity pullback value Δu_{fs} in the free surface velocity history [24,25]. Figures 11 and 12 present examples of experiments for measurements of spall strength for aluminum and iron of various structure and purity. Highly homogeneous single crystals are free of such potential fracture nucleation sites as grain boundaries, inclusions and micro-voids and due to that demonstrate much higher spall strength than that of polycrystalline materials. Impurities in commercial grade aluminum AD1 further decrease the resistance to spall fracture.

Nucleation and growth of the grain-boundary voids are illustrated in figure 13 [28]. The spall surface consists of the dimples which are coalesced pores. Smaller size of dimples at grain boundaries means larger concentration of the damage nucleation sites that facilitates the grain-boundary fracture. It could be expected that the fine-grained materials with larger specific grain surfaces should exhibit a lower resistance to spall fracture. Experiments confirm this expectation, but not always. In particular, refining the grain size by severe plastic deformation is usually accompanied by the spall strength

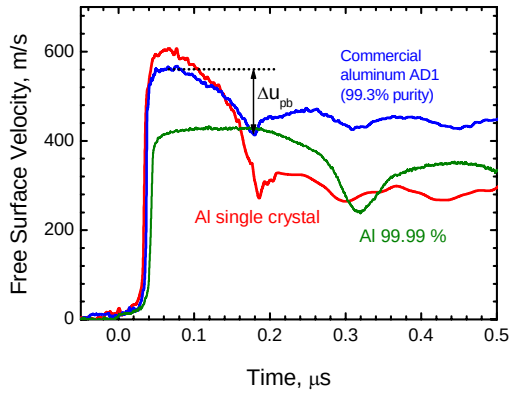

Figure 11. Free surface velocity histories of 2 mm thick samples of commercial aluminum AD1 [26], pure aluminum [21] and aluminum single crystal [19].

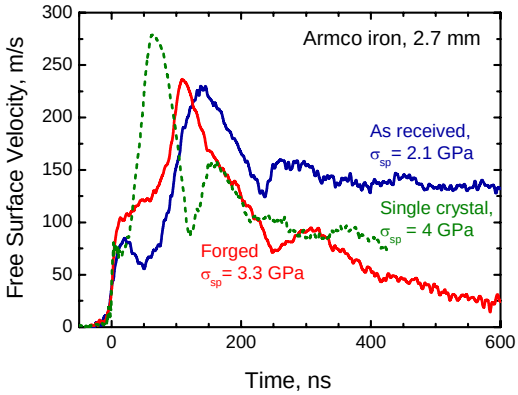

Figure 12. Free-surface velocity profiles of coarse grain (as-received) and fine-grained (forged) Armco-iron samples [27].

growth [27]. Figure 12 presents the example of such effects for Armco-iron. It seems that processing techniques refining the grains results in a redistribution of impurities along larger grain surface.

An ultimate value of tensile stress exists for each condensed matter. The ultimate tensile stress or so called "ideal strength" is equal to the negative pressure at which the bulk modulus is zero. At present, it is possible to perform measurements at a stress level comparable to the ideal strength of condensed material. Figure 14 [3,17] summarizes the spall strength data for aluminum. The results of molecular dynamics simulation of spallation and the *ab initio* calculation of the ideal strength are also shown. The extrapolation to the region of higher strain rates is in agreement with the molecular dynamics calculations and predicts the achievement of the ideal strength at a tension rate of about 2×10^{10} s^{-1}.

Experimentations with large tensile stresses make it important to extend equations of state into the negative pressure region down to real spinodal line at which $dp/dV = 0$. The *ab initio* calculations for this domain correspond to 0 K temperature. Estimations of the temperature dependences of the ideal strength are still very sparse.

Studying the temperature effects is a very natural direction for the development of investigations of time-dependent phenomena under shock-wave loading conditions. The data in figure 6 show that the

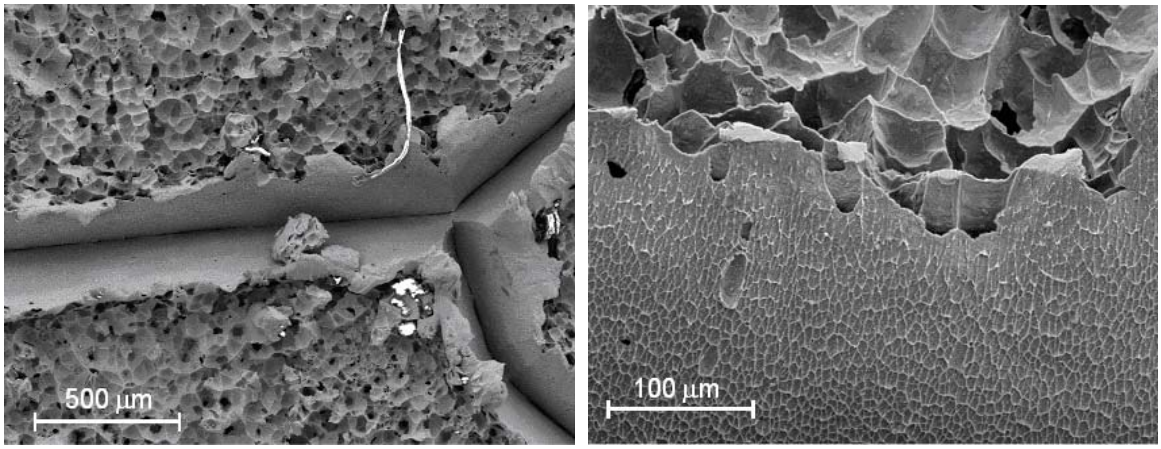

Figure 13. SEM images of the spall fracture surface of Cu+0.1%Si sample in vicinity of grain boundaries [28].

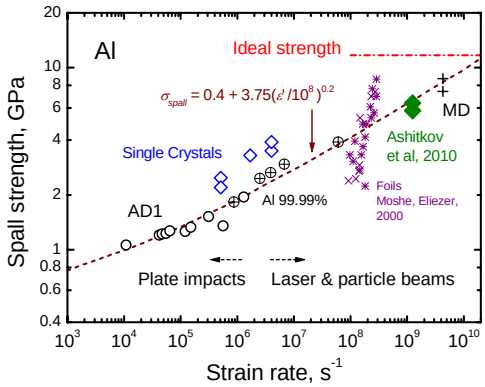

Figure 14. The spall strength of aluminum as a function of strain rate. MD indicates results of the molecular dynamics simulation, "Ideal strength" is a result of *ab initio* calculation. See reference [3] for more details and the sources of data.

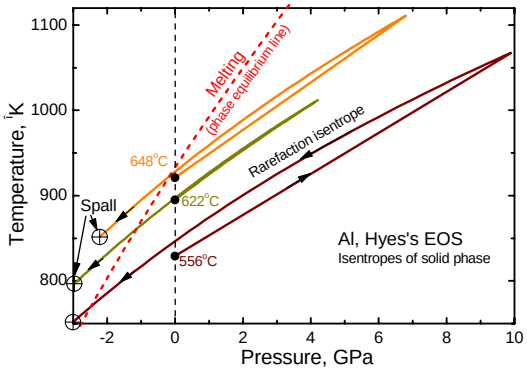

Figure 15. Changes in the state of aluminum under shock compression and subsequent rarefaction for the experimental conditions are indicated in figure 6.

decrease of dynamic tensile strength with heating is much smaller than the strength degradation at the modest strain rates. Dynamic behavior of metals near the melting temperature is of special interest. Figure 15 shows a part of the phase diagram of aluminum calculated for the experimental conditions in figure 6. At high initial temperatures the rarefaction trajectory intersects the melting curve in the negative pressure region. However, traversing the calculated boundary of the melting domain under tensile conditions is not accompanied by any anomalies or a sharp decrease in the tensile strength. The material did not melt, and the measured strength corresponded to the strength of a solid in all cases. If the expected melting did not occur during the high-rate tension at high temperatures, the superheated solid states were therefore realized. The superheat reached 60 – 65 °C for the shortest durations of the shock load.

4. Dynamic strength of hard single crystals and silicate glasses: Failure waves

Whereas the spall strength of ductile metals and alloys greatly exceeds their Hugoniot elastic limit the spall strength of hard ceramics is always much less than the HEL. Unlike ceramics, hard single crystals do not contain such fracture nucleation sites as grain boundaries and may demonstrate very high resistance to spall fracture. Figures 16 and 17 illustrate the mechanical response of c-cut sapphire [29,30]. In the range of the elastic stresses, the sapphire demonstrates an extremely high level of the dynamic tensile strength: the spall strength values vary from 4.2 to 20 GPa depending on the peak stress of shock compression, the load duration and the strain rate. Development of any inelastic deformation leads to complete loss of the resistance to tension in the domain of a sapphire sample where these processes occur. It looks like the damage nuclei may appear in sapphire under both uniaxial compression and following tension and the expectation time for their appearance decreases with increasing both compressive and tensile stresses.

Unlike sapphire, the spall strength of isotropic silicate glasses is high after shock compression both below the HEL and above it. Figure 18 illustrates the response of LK7 borosilicate glass [31]. It is seen in the figure that the reverberation time of mechanical pulse at shock compression below the HEL is much less than that expected for elastic waves. The reason is that the observed second velocity pulse is actually a reflection of the rarefaction wave from a near-surface layer which is not able to sustain tension. In other words, the layer of glass near the impact surface has been failed to the moment when the reflected tensile pulse reached it. Expansion of the cracked layer from the impact surface has been

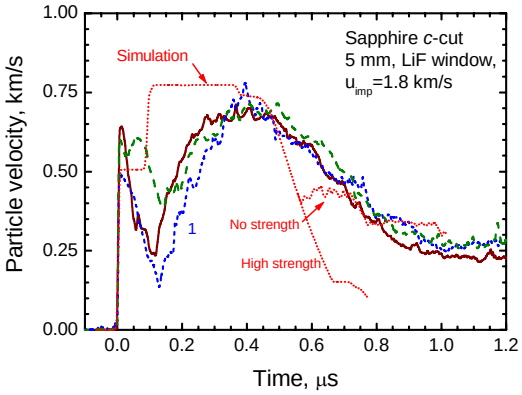

Figure 16. The results of three experiments with 5 mm-thick *c*-cut sapphire samples. Particle velocity histories were recorded at the interface between the sapphire sample and the LiF window [29]. The experimental data are compared with computer simulations assuming a zero or very high tensile strength.

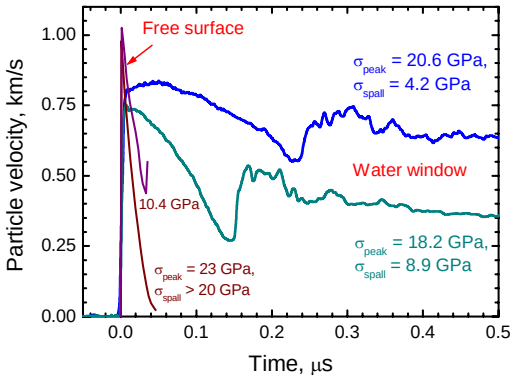

Figure 17. The free surface velocity histories of sapphire samples from the experiments on measurement of the spall strength [30].

treated as propagation of the failure wave. The failure wave is a network of cracks which are nucleated on the surface and propagate into the stressed body.

Since a failure wave nucleates on the glass surface, the magnitude of the leading elastic wave in a shocked specimen consisting of layered glass plates should decrease as a result of its decomposition into two waves at each interface. The decrease of elastic wave amplitude repeats at each interface until the failure threshold is reached. Hence, for a sufficiently large number of layered glass plates, an elastic precursor wave with its amplitude close to the failure threshold could be formed.

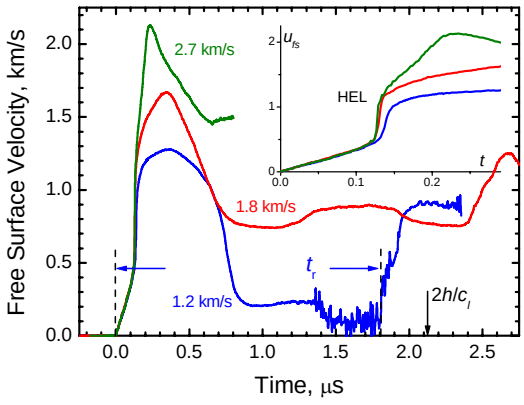

Figure 18. The free surface velocity histories of 6-mm-thick glass plates impacted with different velocities. The inset shows enlarged wave fronts.

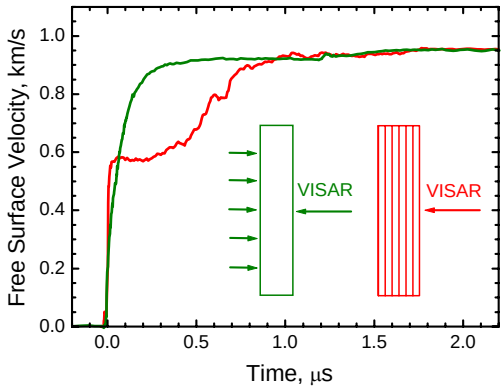

Figure 19. The free surface velocity histories recorded for layered assemblies of 8 soda lime glass plates of 1.2 mm average thickness in comparison with the data for single glass plate 5.9 mm thick.

Figure 19 presents the results [32] of two shots where the free surface velocity histories were recorded for one thick glass plate and layered assemble of eight thin glass plates, subjected to the same impact loading. The shot with a pile shows the waveform that is typical for elastic−plastic solids. The final magnitude of the free surface velocity is practically equal to that of a single glass plate. The response of a layered assembly of thin brittle plates as compared to that of one thick plate is a simple way to diagnose nucleation of the failure process on the plate surfaces and determine the failure threshold. It demonstrates also correctness of our understanding of the failure waves kinematics [32].

The failure waves present a mode of catastrophic fracture in elastically compressed media that is not limited by impact events. It is a regular self-propagating process [33]. One may hope that the investigations of failure waves provide information about the mechanisms and general rules of nucleation, growth, and interaction of the multiple cracks under compression.

5. Conclusions

The presented short summary of our recent experimental data reveals in some cases unusual and exotic behaviour of solids matter under shock-wave loading. Due to extremely short load durations and very high strain rates, approaching the ultimate shear and tensile stresses has been recorded. Earlier such states of materials were realised only in atomistic computer simulations. The experimental observations of strong mechanical metastabilities require new ways to analyse non-linear relaxation to equilibrium and corresponding equations of state. Deep penetration into the negative pressure domain opens a way to investigate the phase transitions and polymorphic transformations under tension and probably allows us to speak about physics of negative pressures. The failure wave presents a new kind of regular fracture mode, studying of which can be useful for understanding earthquake and rock burst processes.

The frontiers of modern physics of shock compression of condensed matter are observable using the unique experimental techniques, such as NIF laser of LLNL, Z-pinch facility of SNL, etc. With these techniques, the exceedingly important unique data about states of matter at extremely high pressures and temperatures have been obtained. The data presented herein have been obtained with standard and relatively inexpensive experimental equipment. The growth of the yield stress with temperature at high strain rates could be expected but was not predicted; for the first time it has been recorded more or less accidentally. The failure wave phenomena in glasses present another example of unexpected findings. It not only explained the existing contradictions in the spall data of different authors for glasses, but also opened the new way of realization of metastable compressive states. All new effects have been uncovered when we just tried to extend parameters of our experiments and to find explanations to all details of experimental observations. This means that there still should be a lot of unusual effects of extremely high strain rates which are waiting for us and everybody may be lucky to uncover one or a few of them.

References

[1] Barker L M and Hollenbach R E 1974 *J. Appl. Phys.* **45** 4872
[2] Bloomquist D D and Sheffield S A 1983 *J. Appl. Phys.* **54** 1717
[3] Ashitkov S I, Agranat M B, Kanel G I, Komarov P S and Fortov V E 2010 *J. Exp. Theor. Phys. Letters* **92** 516
[4] Whitley V H, McGrane S D, Eakins D E, Bolme C A, Moore D S and Bingert J F 2011 *J. Appl. Phys.* **109** 013505
[5] Kanel G I, Razorenov S V and Fortov V E 2004 *Shock-Wave Phenomena and the Properties of Condensed Matter* (Springer) 321
[6] Kanel G I, Razorenov S V and Fortov V E 2004 *Phys. Condens. Matter* **16** S1007
[7] Ashitkov S I, Komarov G I, Agranat M B, Kanel G I and Fortov V E 2013 *J. Exp. Theor. Phys. Letters* **98** 384
[8] Clatterbuck D M, Chrzan D C and Morris J W 2003 *Acta Mater.* **51** 2271
[9] Ogata S, Li J, Hirosaki N, Shibutani Y and Yip S 2004 *Phys. Rev.* B **70** 104104

[10] Clifton R J 1990 *Appl. Mech. Rev.* **43** S9
[11] Meyers M A, Benson D J, Vohringer O et al. 2002 *Mater. Sci. Eng.* A **322** 194
[12] Al'shitz V I and Indenbom V L 1975 *Phys. – Usp*. **18** 1
[13] Duvall G E 1964 *In: Strss Waves in Anelastic Solids*, ed. Kolsky H and Prager W (Springer-Verlag Berlin) 20
[14] Asay J R, Fowles G R and Gupta Y 1972 *J. Appl. Phys.* **43** 744
[15] Chhabildas L C and Asay J R 1979 *J. Appl. Phys.* **50** 2749
[16] Swegle J W and Grady D E 1985 *J. Appl. Phys.* **58** 692
[17] Ashitkov S I, Agranat M B, Kanel G I and Fortov V E 2012 *AIP Conf. Proc.*, **1426** 1081
[18] Kanel G I 2012 *AIP Conf. Proc.* **1426** 939
[19] Kanel G I and Razorenov S V 2001 *Phys. Solid State* **43** 871
[20] Kanel G I, Razorenov S V, Baumung K and Singer J 2001 *J. Appl. Phys.* **90** 136
[21] Zaretsky E B and Kanel G I 2012 *J. Appl. Phys.* **112** 073504
[22] Zaretsky E B and Kanel G I 2013 *J. Appl. Phys.* **114** 083511
[23] Kanel G I, Razorenov S V, Zaretsky E B, Herrman B and Meyer L 2003 *Phys. Solid State* **45** 656
[24] Antoun T, Seaman L, Curran D R, Kanel G I, Razorenov S V and Utkin A V 2003 *Spall Fracture* (Springer New-York) 404
[25] Kanel G I 2010 *Int. J. Fract*. **163** 173
[26] Garkushin G V, Kanel G I and Razorenov S V 2010 *Phys. Solid State* **52** 2369
[27] Garkushin G V, Ignatova O N, Kanel G I, Meyer L and Razorenov S V 2010 *Mech. Sol.* **45** 624
[28] Razorenov S V, Kanel G I, Herrmann B, Zaretsky E B and Ivanchihina G E 2008 *AIP Conf. Proc.* **955** 581
[29] Kanel G I, Nellis W J, Savinykh A S, Razorenov S V and Rajendran A M 2009 *J. Appl. Phys.* **106** 043524
[30] Savinykh A S, Kanel G I and Razorenov S V 2011 *Tech. Phys. Letters* **37** 294
[31] Savinykh A S, Kanel G I and Razorenov S V 2010 *Tech. Phys.* **55** 839
[32] Kanel G I, Bogatch A A, Razorenov S V and Zhen Chen 2002 *J. Appl. Phys.* **92** 5045
[33] Kanel G I 2006 *AIP Conf. Proc*. **845** 870